ELSEVIER

Chemical Physics 272 (2001) 243–258

Chemical Physics

www.elsevier.com/locate/chemphys

A simulation of naphthalene matrix isolation: comparison with experiments

C. Crépin [a,*], P. de Pujo [b], B. Bouvier [b], V. Brenner [b], Ph. Millié [b]

[a] *Laboratoire de Photophysique Moléculaire, CNRS, Université Paris-Sud, Bât. 210, 91405 Orsay Cedex, France*
[b] *Laboratoire de Chimie Théorique, DSM/DRECAM/SPAM, CEA-Saclay, 91191 Gif sur Yvette Cedex, France*

Received 13 March 2001; in final form 30 July 2001

Abstract

The trapping of a naphthalene molecule in an argon matrix is simulated using an original method based on classical molecular dynamics calculations. A numerical simulation of the gas mixture deposition on a cold argon surface reproduces the matrix growing process. Three main trapping sites are obtained. The naphthalene replaces four or five argon atoms in the (1 1 1) crystallographic plane, or four argon atoms in the (0 0 1) crystallographic plane of the fcc argon lattice structure. The simulated structures are correlated to experimental site effects: the spectroscopic and dynamic molecular properties depend only on the lattice plane occupied by the naphthalene. © 2001 Elsevier Science B.V. All rights reserved.

Keywords: Molecular dynamics; Numerical simulations; Naphthalene; Argon solid; Matrix isolation; Site geometry; Site effects

1. Introduction

Matrix isolation techniques have been widely used to study spectroscopic properties of isolated molecules in an inert medium, which acts as a weak solvent and induces only a small perturbation of the electronic structure of the guest molecule. This leads to shifts and broadening of lines in the electronic spectrum of the free molecule. Different geometric structures of the trapping sites induce an inhomogeneous broadening because of the site dependence of frequency shifts. The fluorescence-line-narrowing technique allows a site selection, getting rid of a part of inhomogeneity. Crépin and Tramer have realised such experiments with naphthalene molecules embedded in cryogenic solids and observed site effects on the spectroscopic and dynamic molecular properties of excited molecules [1]. Unfortunately, no experimental techniques determining the geometric structure of these sites are available. The only solution is numerical simulations.

The first attempt to simulate naphthalene–rare gas systems, performed by Najbar et al. [2], used a very simple approach. These authors studied the energy relaxation by an insertion method of a naphthalene molecule with some, one by one, added atoms in a cavity built inside a rigid matrix. It appears difficult to determine by this method the site structures of the lowest energy because no

* Corresponding author. Tel.: +33-1691-57539; fax: +33-1691-56777.
E-mail address: claudine.crepin-gilbert@ppm.u-psud.fr (C. Crépin).

0301-0104/01/$ - see front matter © 2001 Elsevier Science B.V. All rights reserved.
PII: S0301-0104(01)00468-2

motion of atoms of the matrix was possible and no precise potentials for describing the interactions between particles were available at this time. More recently, a new solution has appeared for molecular dynamics (MD) calculations where the classical mechanics trajectories for each particle are calculated to study specific processes. For instance, Fraenkel et al. [3] used this technique to study the site formation of anthracene molecules deposited in an argon matrix with two simulation approaches. The first is based on an insertion method followed by a relaxation where all degrees of freedom are permitted to change. The other one consists in a growth of the matrix from a prefabricated template. The growth method was also chosen by Cruz and Lopez [4] for spherical species in an argon matrix.

We have used the MD method in our work to build a fcc argon crystal containing a molecular impurity. We focus our attention on a close reproduction of experimental conditions as, for instance, the equilibrium temperature and the dissipation of the excess energy arising from gas condensation. In this way the landing of the particles and the relaxation processes have been examined carefully. This method has then been applied to the naphthalene molecule as the impurity in order to determine the geometrical site structures in an argon matrix. We have chosen argon atoms in our simulations because of very stimulating experimental data obtained in matrices (described in part I [1]) and in small clusters [5]. Moreover, new potentials for the weak interaction between a naphthalene molecule and an argon atom are evaluated by Troxler and Leutwyler [5].

The paper is organised as follows: first the simulation method is described, the results of calculation are then analysed and compared to experimental data. An assignment of calculated site structures and observed site properties is proposed.

2. Conditions of simulation

This work is based on the simulation of the matrix formation by modeling, at the molecular scale, the condensation process of a low-pressure gas on a surface maintained at a low temperature. This is achieved by MD calculations reproducing the growth of a germ which has the geometrical properties of the crystal. The molecule is considered as a rigid body. Its location and orientation in a space-fixed system of axis are described by three Cartesian coordinates giving the location of the centre of mass of the molecule and four quaternions giving the orientation of the molecule around its centre of mass. No constraints have been used. The integrator algorithms used are a Verlet-velocity form to solve the translational differential equations and a ''leapfrog'' proposed by Fincham to solve the rotational differential equations. The coupled differential equations of motion and the numerical algorithm are described in detail in Ref. [6]. The interatomic potentials are Lennard-Jones (LJ) pair potentials taken from Ref. [5]. It is well known [7] that LJ potentials do not allow the fcc structure of a pure rare gas solid to be obtained by simply cooling a drop or compressing a gas. This is due to solid effects that LJ potentials, as well as any two-body potential expressed by terms of $(1/r)^n$, cannot reproduce, unless the crystal grows from a prefabricated fcc germ under certain conditions. This behaviour may be due to many-body terms but in the case of argon atoms we have verified that it is not a triple-dipole effect.

We used this MD technique for constructing a pure fcc lattice nucleus by gas deposition with the following simulation protocol: a rectangular box is filled with four argon layers according to the fcc lattice and parallel to the xOy plane of the space-fixed system of axis. The atoms of the lowest layer are fixed in space in order to avoid translational and rotational motion of the lattice during the growth process and the transformation of the initial fcc germ into a near spherical cluster. The second layer is used as a thermostat: at regular time intervals of the MD run, the velocities of all atoms of the layer are rescaled to force the atoms toward a desired temperature as described in Ref. [8]. The atoms of the last two layers can move freely under action of the interaction forces. A MD run is performed to heat the germ to the working temperature before starting the gas deposition. Then, at regular time intervals, an argon

atom is shot at the upper layer with an initial thermal velocity. The atom is captured after collision with the surface; the collision energy is transferred to the surface and then dispersed in all degrees of freedom of the lattice [9]. The initial (x, y) Cartesian coordinates are chosen randomly in a rectangle slightly smaller than the dimensions of the upper layer. The initial translational velocity is oriented parallel to the Oz axis. For convenience the perpendicular velocity component is taken equal to zero, but this feature is compensated for the undulating surface nature [6,9]. This allows an efficient random spraying of the surface without loss of atoms. The lattice growth is thus obtained with the collision of about 500 adatoms.

No periodic conditions are used but a cut-off distance of 15 Å is applied. To discard possible artefacts due to edge effects, we chose an upper layer large enough to avoid the interactions between a particle evolving in the vicinity of the layer centre and edge atoms. In that case the surface is a square of 40×40 Å^2. In the same way, it was verified that a depth of four layers is more than enough by calculating the interaction energy for a particle moving at the surface of the germ as a function of the number of successive layers. The choice of the initial velocity of adatoms corresponds to the argon mean velocity (500 m s^{-1}) in a gas at 300 K. For a realistic description of the deposition process, one has to take experimental values into account. The deposition velocity is 1 mmol h^{-1} cm^{-2}. At the molecular scale, this corresponds in average to the arrival of one particle per 40 μs on the surface; this rate cannot be reproduced by MD calculations. In fact the most pertinent parameter is not really the deposition velocity but rather the lattice relaxation time, i.e. the length of time the lattice needs to dissipate the whole collision energy in its internal degrees of freedom after each collision. Dynamical tests based on the temperature evolution of the sample have shown that the relaxation time is around 100 ps at a thermostat temperature of 25 K. Most simulations were made at 25 K, while several ones were made at 10 K. A lower temperature leads to more frozen configurations and the production of less stable sites. A temperature of 25 K was preferred in order to obtain only the most stable sites. As a precaution and without penalizing strongly the computer time, a value of 200 ps was retained between the deposition of two particles. We notice that this time interval is distinctly larger than the one used in Refs. [3,4]. We used an integration time step of 10 fs and this assures, during a MD calculation, a relative stability of the energy better than 10^{-6} at constant total energy.

The last point concerns the structure of the initial lattice germ. We have selected two different germs, each one with layers corresponding to one of the crystallographic planes (0 0 1) and (1 1 1) of the fcc lattice. The basic idea is that fcc growth may be favoured or not according to a specific crystallographic plane. This is estimated in a plot of the energy contour surface of, for instance, an argon atom moving at a constant distance from the upper layer. In the case of the (1 1 1) crystallographic plane (Fig. 1), the well depths of different possible sticking sites have very similar values. According to the impact, the atom will then move

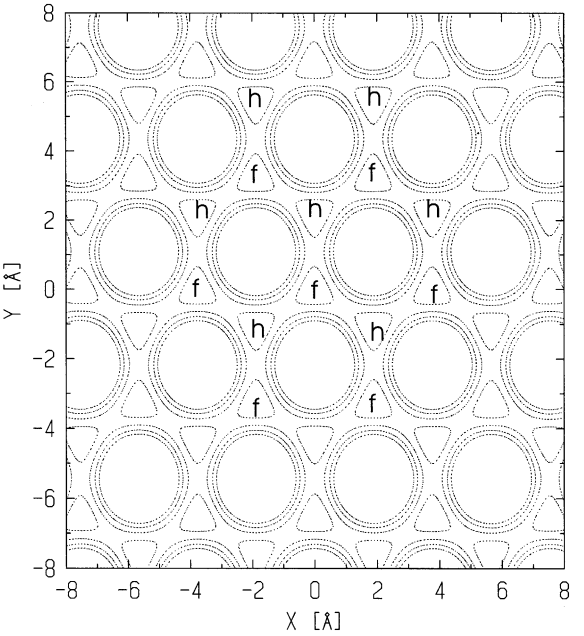

Fig. 1. Contour map of the potential energy of an argon atom at a constant distance above the surface of a (1 1 1) plane of an fcc argon lattice of four layers; *h*: potential wells for an adatom initiating a hcp structure, *f*: potential wells for an adatom following the fcc structure.

into a fcc well or into a hcp well and thus the nature of the growth will be modified. This is not the case with a (0 0 1) plane where all wells allow only fcc growth. This is the reason of our choice of the (0 0 1) plane.

In these simulation conditions, the deposition of argon atoms with a starting germ of the (0 0 1) type leads to a well-ordered crystal with no defects or vacancies in its central part. We just note a few troubles with atoms on the edges where the structure of the solid cannot be reproduced in absence of periodic image conditions. Because of the short range interactions and the cut-off radius, these effects are totally negligible for energetic and stabilisation of species trapped near the centre of the solid. The deposition of argon atoms with random impact points induces a lattice growth that is not far from layer by layer (Fig. 2).

The naphthalene molecule is inserted into the sequence of adatoms as follows: first, about a 100 argon atoms are shot randomly at the surface in the same way as for the pure lattice. This process creates faults on the perfect surface before the projection of the naphthalene molecule in the vicinity of the surface centre. The naphthalene is supposed to be rigid and planar as given in Ref. [10]. The molecule starts initially oriented parallel or perpendicular (two extreme angular orientations) to the xOy plane and reaches the surface. As in Ref. [6] no initial rotational velocity is given to the molecule. With or without rotation, the nature of the shock remains unchanged, only the point of impact of the molecule will be different but it will not modify the relaxation of the molecule on the lattice. As naphthalene is planar, it will be embedded in a crystallographic plane. As in the case of argon atom deposition, the naphthalene molecule is captured by collision with the surface. The simulation clearly shows that after the collision the molecule does not remain at its impact point but moves randomly. For example, if the molecule is "falling down" on the neat upper (0 0 1) layer of the initial germ, there is very fast diffusion on the surface. Fig. 3 shows the trajectory of the mass centre of the molecule on the neat surface during 5 ns. This high mobility on the lattice surface is to be compared with that of N_2O molecules on large argon cluster surfaces [6]. The naphthalene molecule arriving after deposition of a 100 argon atoms collides with a rather chaotic surface so that its diffusion is slackened. Nevertheless, the probability of finding a planar area in the (0 0 1) crystallographic plane remains high. The process of diffusion stops only when several argon atoms start to surround the naphthalene molecule.

In order to perform statistical analysis, only about 60 simulations of the deposition have been realised in view of the very long computer times.

The argon atoms arriving after the deposition of the molecule are trapped preferentially in sites

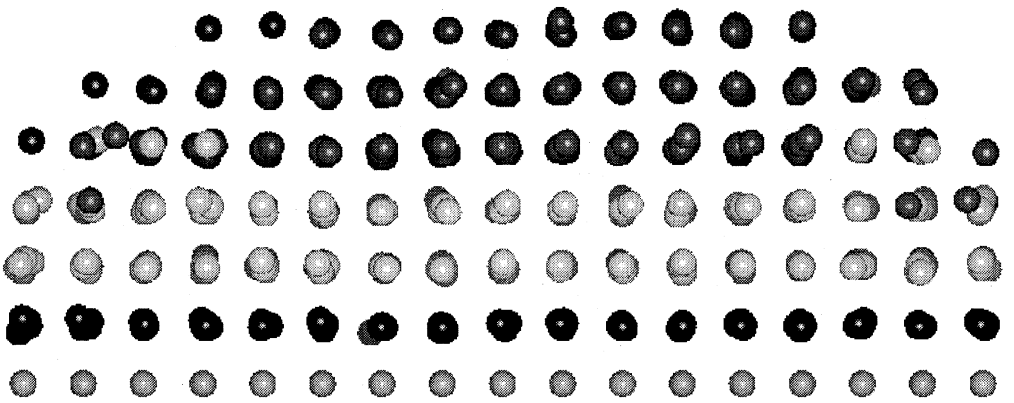

Fig. 2. Simulated deposition of 200 argon atoms on the initial four (0 0 1) layers argon block in the (xOz) projection at 25 K—initial argon layers are (xOy) planes; first layer (light grey): fixed atoms, second layer (dark grey): argon maintained at 25 K; third and fourth layers (light grey): free atoms of the upper layers of the initial germ; upper layers (dark grey): deposited atoms.

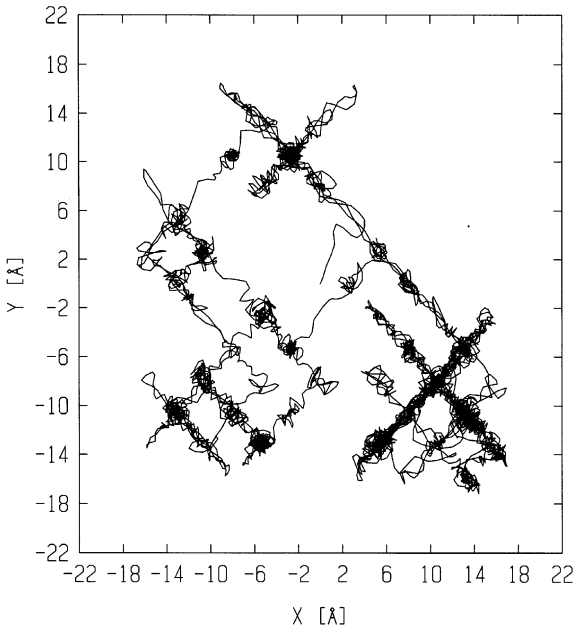

Fig. 3. Trajectory of the centre of mass of the naphthalene on the surface maintained at 25 K of a four (0 0 1) layers argon block during 5 ns.

surrounded by argon atoms and the covering of the molecule by complete argon layers needs the additional deposition of 400–500 argon atoms. It is a consequence of the differences in the interaction energies E_{int} of the different pairs of atoms: $E_{int}(Ar–Ar) > E_{int}(Ar–C) > E_{int}(Ar–H)$ [5] (Table 1)—the equilibrium distances being of the same order of magnitude for the three pairs of atoms. This is in agreement with experiments and simulations on naphthalene–Ar_n clusters [5] where non-wetting clusters were preferentially formed.

The complete incorporation of the guest molecule in the lattice needs very long calculation times and the simulation of the gas deposition is stopped when one or two argon layers cover the molecule.

Table 1
LJ pair potentials used in this work, from Ref. [5]

	Ar–Ar	Ar–C	Ar–H
ε (K)	142.1	57.636	25.674
σ (Å)	3.36	3.385	3.207
R_{min} (Å)	3.77	3.80	3.60

This is sufficient to characterise the geometry of the sites. In order to discuss the energetic considerations (see Section 3.2), we have built thicker argon samples where the naphthalene molecule is trapped in the configurations obtained by the simulation of the gas deposition. These samples will be denoted here after "model" configurations.

3. Results and discussion

3.1. Site geometries

The predominant site geometry corresponds to the molecule trapped in the (0 0 1) crystallographic plane. Only one site (the I(0 0 1) configuration) represented in Fig. 4 is obtained. The molecule replaces four argon atoms in the (0 0 1) plane (Fig. 4c) without any strong perturbation of this layer. The perturbation of the fcc argon lattice resulting from the presence of the molecule affects mainly the nearest upper and lower layers (Fig. 4a). The distance between (0 0 1) layers in the pure fcc argon lattice (2.58 Å) is much smaller than the equilibrium distances of the C–Ar or H–Ar given by the model LJ pair potentials (3.80 and 3.60 Å respectively). One can see in Fig. 4d that four argon atoms in each nearest layer lie just underneath or above hydrogen atoms, a fifth argon atom being underneath or above the centre of mass of the molecule, very close to carbon atoms: C–Ar distances of 3.33 and 3.34 Å are found while some H–Ar distances reach 3.03 Å. These X–Ar distances (X = C or H) are shorter than the corresponding σ(X–Ar) parameters of the pair potentials (see Table 1), then the repulsion plays a very important part in the interactions. This explains the distortion of the two nearest layers.

Other sites exhibit the molecule trapped in the (1 1 1) crystallographic plane. This result is very interesting. First of all, it means that the geometry of the initial germ does not prevent the molecule for finding different sites. Secondly, as the usual growth of the fcc lattice is (1 1 1) layer by (1 1 1) layer [7]—(1 1 1) planes are the most dense crystallographic planes of the fcc lattice—this kind of sites is commonly assumed without any corroboration from calculations. In the work of Najbar

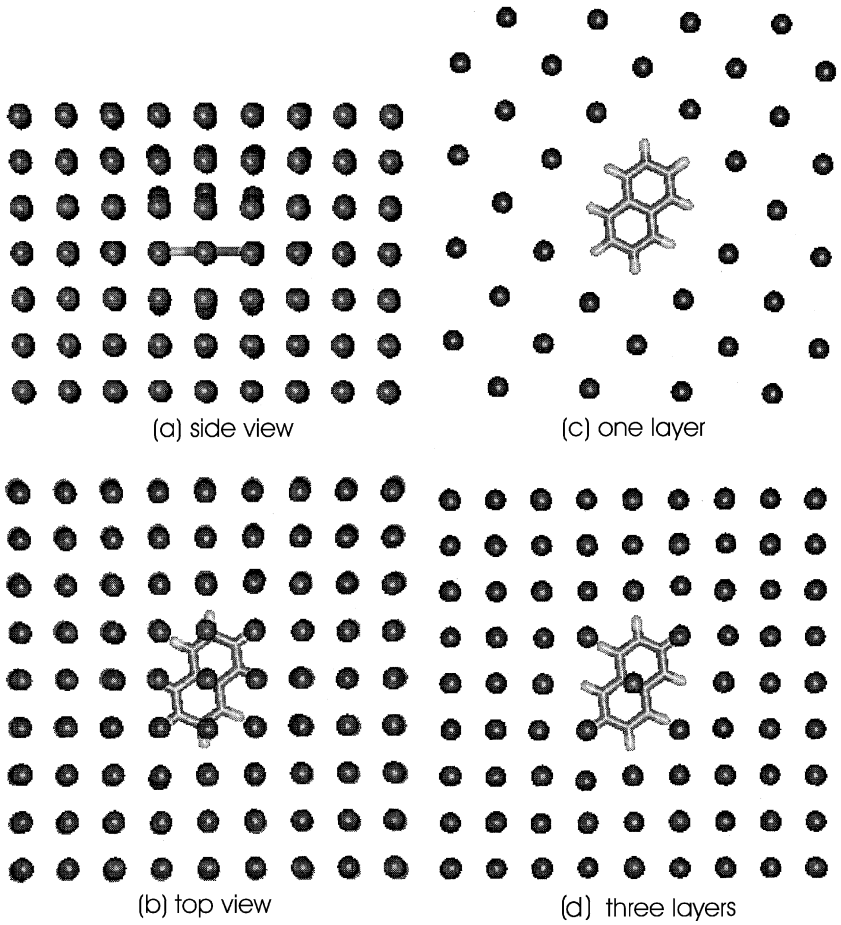

Fig. 4. The I(0 0 1) configuration: side view (a) and top view (b) of the model doped argon lattice; (c) the (0 0 1) plane occupied by the naphthalene; (d) top view of three (0 0 1) planes: (c) and planes above and below the molecule.

et al. [2], the molecule was supposed to be embedded in this plane, replacing six or seven argon atoms. In our simulations, the cavities are much smaller: we found two different configurations where the naphthalene replaces four or five argon atoms (I(1 1 1) and II(1 1 1) configurations, respectively), represented in Figs. 5 and 6. In both cases, the upper and lower (1 1 1) layers are not strongly disturbed (Figs. 5a and 6a). As shown in Figs. 5d and 6d, the nearest argon atoms in these layers are not directly above or below any carbon or hydrogen atoms. Moreover, the distance between (1 1 1) layers is larger than that between (0 0 1) layers (3.02 Å in comparison with 2.58 Å). The shortest C–Ar distances measure 3.40 and 3.44 Å. The main perturbations in the fcc argon lattice affect the nearest argon atoms in the same crystal layer. In the smallest trapping site (the I(1 1 1) configuration, Fig. 5), there are just four argon atoms, indicated by a star in Fig. 5c, which have an important displacement in comparison with their positions in the pure Ar crystal. The II(1 1 1) configuration corresponds to the elimination of one of these four atoms (Fig. 6c). Nevertheless, in these two configurations, the repulsive part of the pair potentials is also reached.

In order to determine the influence of the initial germ structure, we have simulated the gas deposition on another crystallographic plane of the fcc lattice, the (0 1 1) plane. The molecule is never

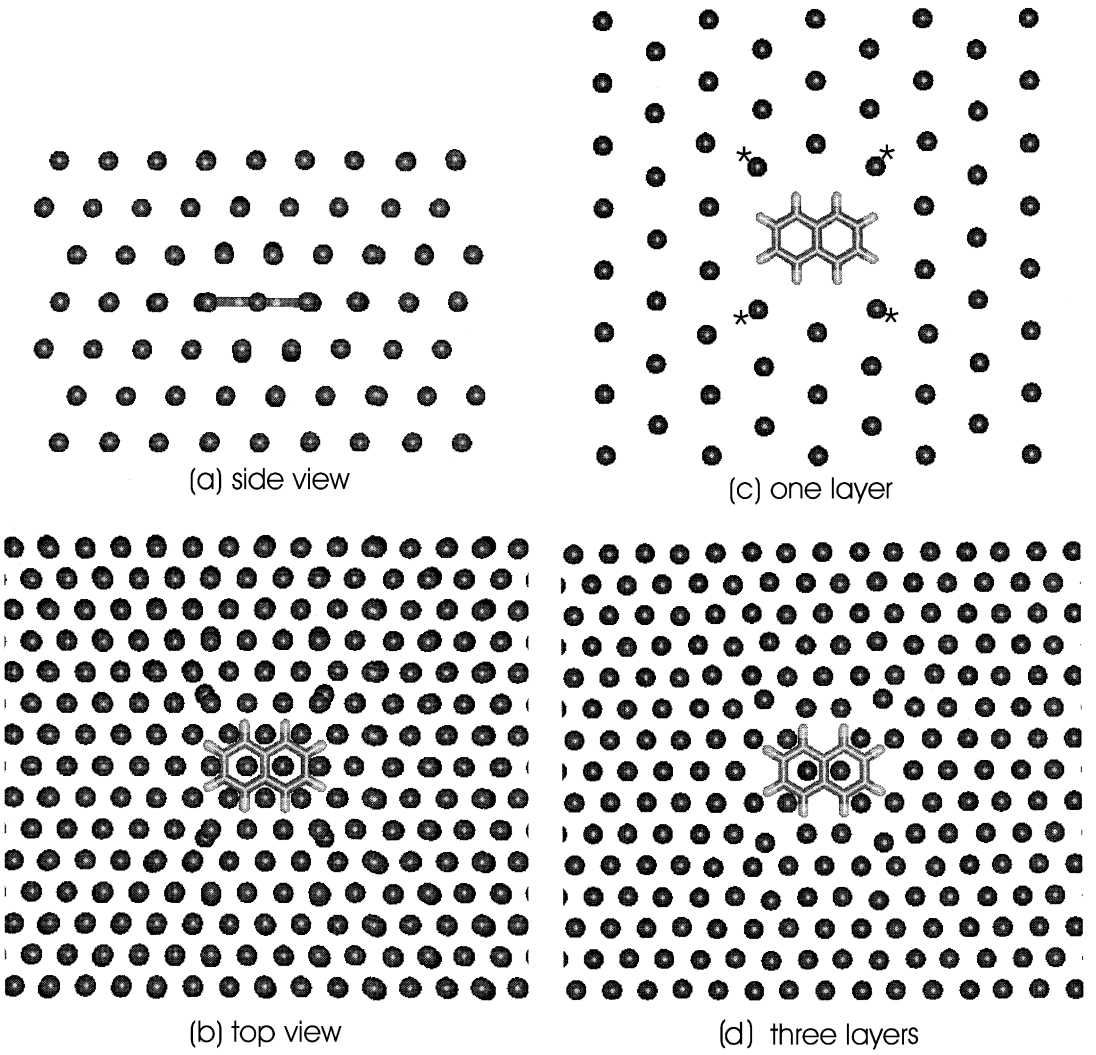

Fig. 5. The I(1 1 1) configuration: side view (a) and top view (b) of the model doped argon lattice; (c) the (1 1 1) plane occupied by the naphthalene, ∗: see text; (d) top view of three (1 1 1) planes: (c) and planes above and below the molecule.

found to lie on the (0 1 1) plane so that these initial conditions do not strongly influence the final configurations. As a matter of fact, we have always found the molecule embedded in the (0 0 1) or (1 1 1) crystallographic planes, with preponderance for the (1 1 1) plane. In the case of the (0 0 1) plane, only the I(0 0 1) configuration described above was obtained whereas in that of the (1 1 1) plane, the I(1 1 1) and II(1 1 1) configurations were obtained. Thus, three main trapping sites are found whatever the initial conditions.

In the three main configurations, the perturbations of the fcc argon lattice are localized around the guest molecule. All the argon atoms are located very close to their positions in the neat argon lattice: these positions are the most stable ones even in the neighbourhood of the molecule because of the interaction with all the argon atoms of the lattice. Larger trapping cavities have never been obtained. This means that the energy loss resulting from the elimination of an extra argon atom is too large to be compensated by a more "comfortable"

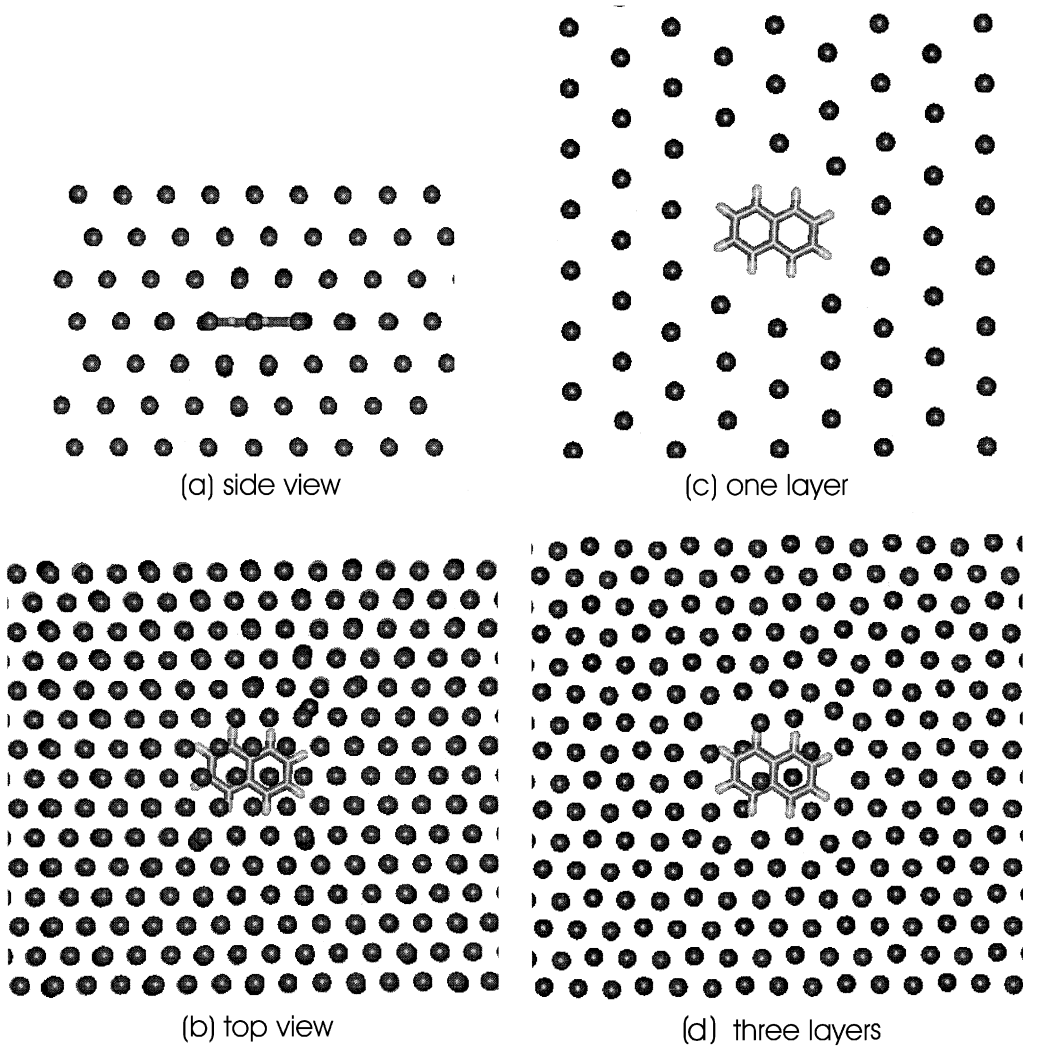

Fig. 6. The II(1 1 1) configuration: side view (a) and top view (b) of the model doped argon lattice; (c) the (1 1 1) plane occupied by the naphthalene; (d) top view of three (1 1 1) planes: (c) and planes above and below the molecule.

site for the guest molecule. Calculations presuming a larger site for the guest molecule inside a (1 1 1) crystallographic plane, as described in Ref. [2], confirmed this assumption. The interaction energy E_I between the molecule and the whole Ar lattice in the different sites decreases at 10 K by ~170 K in both sites where the molecule replaces six argons and by an additional ~300 K with naphthalene in a seven argon atoms cavity, whereas the interaction energy of a neighbour argon atom with the lattice is around −1400 K (we have also verified that E_I increases in larger cavities). Najbar et al. [2] have obtained larger vacancies than us because their method did not take into account the relaxation of the lattice and because they used different pair potentials, their C–Ar potential being very close to the Ar–Ar one.

Furthermore, we performed MD calculations on samples with larger trapping cavities. They show that these cavities remain as they have been initially built, even after an annealing at 35 K for as long as 30 ns. Realistic annealing times cannot

be simulated but these results show that an a priori assumption of a cavity size can lead to artefacts. It may also be related to the experimental fact that in argon matrices, all the unstable sites that result from non-perfect deposition conditions cannot be totally eliminated by annealing [1].

The existence of three main sites for the naphthalene trapped in an argon matrix was thus confirmed. Secondary sites are sometimes obtained, especially by simulating a deposition on a colder surface (10 K instead of 25 K), but they are not discussed.

3.2. Energetic of the main sites

In the model samples (Section 2) corresponding to the three main configurations, the molecule is covered by four or five argon layers and edge effects are negligible. The model samples include 11 (0 0 1) layers for the I(0 0 1) configuration (1586 argon atoms) and 9 (1 1 1) layers in other cases (1289 or 1288 argon atoms). Such a sample containing only one molecule is equivalent of the experimental matrix isolation where a $C_{10}H_8$/Ar ratio less than 1/1000 was used. Model samples have been annealed at 25 K for several nanoseconds before cooling down to 0.1 K in order to obtain the fixed configurations. Characteristic energies of the three configurations were then calculated: E_I, the energy of interaction between the molecule and all the argon atoms of the lattice (Table 2), and E_T, the potential energy of the whole sample.

The energies of the interaction between the naphthalene and Ar atoms contained in the nearest upper or lower layer (calculated at 0.1 K) and those between the molecule and the argon atoms of the same lattice layer, calculated under the same conditions, are reported in Table 2 for the three configurations. These evaluations confirm that E_I is essentially determined by the interaction of the molecule with the rare gas atoms lying over and under it. The effect of the second upper and lower layers on E_I is not negligible in the case of the I(0 0 1) configuration. The variations of these energies from one structure to another seem to be mainly related to the repulsive forces between the guest molecule and the host atoms, either in the same lattice layer (stronger in the I(1 1 1) and II(1 1 1) configurations) or between the layers (stronger in the I(0 0 1) configuration).

Table 2
Interaction energies (K) between the naphthalene and the lattice—precision in ( )—calculated at 0.1 K

Interaction energy	Site		
	I(001)	I(111)	II(111)
E_I	−7440 (2.5)	−7781 (2.4)	−7947 (2.4)
E_N	−2334	−2880	−2910
E_M	−1330	−1017	−1128
E_L	−1442	−1004	−999

The total interaction energy E_I (first row) is the sum of all the X–Ar interaction energies, X being an atom of the naphthalene molecule and Ar an argon atom of the model sample. E_I is decomposed in the different contributions (three last rows) of the different lattice layers surrounding the molecule: nearest upper or lower layer (E_N), argon layer occupied by the molecule (E_M), all the other layers (E_L).

The overall interaction energies corresponding to the I(1 1 1) and II(1 1 1) configurations are close. The small difference comes from a weaker repulsion with the argon atoms included in the layer containing the molecule in the larger cavity, as shown by the analysis of E_I. In the case of the molecule in the (0 0 1) plane, E_I is clearly higher. As model samples for I(0 0 1) and X(1 1 1) (X(1 1 1) = I(1 1 1) and/or II(1 1 1)) configurations have different geometries and do not contain the same number of argon atoms and layers, edge effects could affect global energies in different ways. In order to compare the three configurations, the potential energies E_P^b of argon blocks surrounding the trapped molecule, embedded in the whole model samples, have been calculated. The size of these argon blocks is chosen in such a way that the distance between any atom of the guest molecule and the external argon atoms is larger than the cut-off distance. Calculations are performed at 0.1 K with fixed geometries and a cut-off distance of 10 Å. Similar calculations on neat argon blocks of the same size lead to reference energies E_P^0. The doped crystals have always slightly higher potential energies than neat argon crystals by about 5%. The results on E_I and characteristic energy differences ΔE are reported in Table 3: $\Delta E = (E_P^b - E_P^0)/N$ with neat argon blocks of N argon atoms. In spite of a better local stabilisation of the molecule

Table 3
Interaction energy (K) (E_I with the ground state geometry and E_I^* with excited state geometry of naphthalene), differential energy by particle (ΔE)—see text, interaction energy differences ($\Delta E_I = E_I^* - E_I$), in the three model structures at 0.1 K

Configuration	Geometry					
	S_0		S_1[a]		T_1[a]	
	E_I	ΔE	E_I^*	ΔE_I	E_I^*	ΔE_I
I(0 0 1)	−7440	74	−7380	60	−7363	77
I(1 1 1)	−7781	76	−7700	81	−7766	15
II(1 1 1)	−7947	81	−7870	77	−7933	14

[a] Energies obtained with modified molecular geometries without a relaxation of the lattice, using pair potentials of the ground state.

in the larger cavity E_I (I(1 1 1)) > E_I (II(1 1 1)), the perturbation of the argon lattice is smaller in the case of the smaller cavity: ΔE(I(1 1 1)) < ΔE(II(1 1 1)). The system is slightly better stabilised in the I(0 0 1) configuration: ΔE(I(0 0 1)) < ΔE(I or II(1 1 1)). We conclude that the three configurations are nearly isoenergetic: energy differences between the three ΔE are smaller than kT, at the lattice temperature T.

Our results may be compared to the recent MD simulations on anthracene in solid argon [3]. Both trapped molecules are planar and the interactions with the matrix are similar. The anthracene sites correspond also to the trapping of the molecule in the (0 0 1) and/or (1 1 1) planes of the fcc lattice. This confirms that only these two crystallographic planes are involved in the trapping of such species. In the smallest cavities, the anthracene takes the place of six argon atoms, in agreement with the smallest cavities found in this work for the naphthalene: molecules are squeezed in their trapping sites. More than three trapping sites were found for the anthracene: the number of sites is more limited in our simulations than in Ref. [3] because our deposition and cooling rates are slower and thus metastable sites are not stabilised.

4. Comparison with experiments

4.1. Summary of the main experimental results

The detailed results are described in part I [1]. For this discussion, we just recall their principal features. Two main families of sites, named A and B in part I, have been observed in argon matrices. Their spectra and decay times differ in the following ways:

i. the $S_1 \leftrightarrow S_0$ origin frequencies are 31,860 cm^{-1} for site A and 31,900 cm^{-1} for site B (corresponding to 32,018 cm^{-1} in the isolated molecule [11]),
ii. the $S_1 \rightarrow S_0$ fluorescence spectra show different vibronic intensity distributions: the intensity ratios $I(0_0^0)/I(\text{“}b_{1g}\text{”})$ and $I(\text{“}a_{1g}\text{”})/I(\text{“}b_{1g}\text{”})$ are larger for site B than for site A (a_{1g} and b_{1g} are short notations for vibronic bands involving totally symmetric a_{1g} modes and non-totally symmetric b_{1g} modes, respectively),
iii. the fluorescence lifetimes τ_{fl} are different: $\tau_{fl}(A) = 24$ ns and $\tau_{fl}(B) = 90$ ns,
iv. the phosphorescence to fluorescence intensity ratio upon S_1 excitation is higher for site A than for site B; this is related to (iii) if we assume that the shortening of τ_{fl} results from a more efficient intersystem crossing,
v. the $T_1 \rightarrow S_0$ origin frequencies are 21,205 cm^{-1} in A and 21,370 cm^{-1} in B (corresponding to 21,398 cm^{-1} in the gas phase [12]),
vi. the phosphorescence bands are broad for site B (125 cm^{-1}) whereas they are roughly as narrow as fluorescence bands for site A (20 cm^{-1}).

4.2. Assignment

The differences observed between both families of sites are not very large and much more theoretical work is needed, especially on the excited electronic states, for the quantitative analysis. Nevertheless, a reasonable assignment can be derived from a comparison of experimental and simulated data.

First of all, the probabilities to find different configurations cannot be deduced from a limited number of simulations. The probability to find the I(0 0 1) one is artificially enhanced in our simulations by the choice of the initial (0 0 1) surface whereas in reality, the X(1 1 1) configurations could be favoured by a crystal growth involving the formation of successive (1 1 1) layers. From an energetic point of view (Table 3 and Section 3.2),

all three configurations are equally probable. Three calculated geometries correspond to only two well-defined families of sites deduced from experiments. It suggests that two of the three simulated configurations have similar spectroscopic and dynamic properties. Since the $S_1 \leftrightarrow S_0$ and $T_1 \leftrightarrow S_0$ transitions involve a $\pi \rightarrow \pi^*$ electron promotion, the important interactions concern σ-type orbital overlaps with the 3p orbitals of argon atoms contained in the layers above and below the molecular plane and π-type orbital overlaps with the same 3p orbitals of argon atoms in the same layer as the molecule. For the nearest neighbours, mean Ar–C distances between different layers are shorter than in the same layer and σ-type overlaps are more important than π-type ones. A larger difference between the I(0 0 1) and X(1 1 1) sites than between I(1 1 1) and II(1 1 1) ones is then expected. The A and B families of sites should correspond to the I(0 0 1) and X(1 1 1) configurations. We suggest that the I(0 0 1) geometry corresponds to the A-site and the X(1 1 1) geometry to the B-site. The main reasons for this assignment are the following.

The intersystem crossing rate is larger for the A than for the B family (features (iii) and (iv)). Different models [13–19] proposed in order to describe the "borrowing" of the spin–orbit coupling strength resulting from the external heavy atom effect (EHAE) predict the medium-induced spin–orbit coupling term roughly proportional to the overlap integral of the excited π^* orbitals of the molecule with the rare gas atomic orbitals. Therefore, the efficiency of EHAE should depend on the average distance between the C atoms and the argon atoms. Obviously, this distance is smaller and the interaction stronger in the I(0 0 1) than in the X(1 1 1) configurations whereas the difference between I(1 1 1) and II(1 1 1) configurations is small.

A similar conclusion may be deduced from the red-shifts of the $S_1 \leftrightarrow S_0$ and $T_1 \rightarrow S_0$ transitions with respect to the gas phase. The red-shift results from a less repulsive or a more attractive interaction with the host atoms in the excited than in the ground state. Usually, attractive dispersive interactions are enhanced in the excited state because of a larger polarisability of the molecule. The stronger red-shift in the A family of sites (features (i) and (v)) should then correspond to the stronger interaction between π^* electronic orbitals and host orbitals in the excited states, suggesting the assignment of the A-site to the I(0 0 1) configuration.

The feature (vi) is also a key point to the assignment of the different configurations. Broad phosphorescence bands can be explained either (a) by a more or less pronounced modification of the site geometry during the long lifetime of the triplet state or (b) by an absence of correlation between the shifts of $S_1 \leftrightarrow S_0$ and the $T_1 \rightarrow S_0$ transitions induced by the environment. In the X(1 1 1) configurations, the molecule is less squeezed between two lattice layers than in the I(0 0 1) configuration and a small rotation out of the (1 1 1) plane is not excluded. As a matter of fact, simulations show that the molecular plane presents a small angle (∼1°) with the (1 1 1) plane in the X(1 1 1) case whereas no significant deviation of the molecule from the (0 0 1) crystallographic plane is found in the I(0 0 1) case. We have thus some distribution of orientations in X(1 1 1) sites: their effect on $S_1 \leftrightarrow S_0$ and $T_1 \rightarrow S_0$ transitions may be different. Within a class of molecules with $\nu(S_1\text{–}S_0) = \nu$(laser), the frequencies of the $T_1 \rightarrow S_0$ transition may be not identical. In addition, during the triplet lifetime, a slight molecular motion is not excluded in the X(1 1 1) sites (rotation in the X(1 1 1) and translation in larger II(1 1 1) configurations). Broad bands in the phosphorescence spectrum would come from fluctuating structures (B family ↔ X(1 1 1) configurations) and narrow bands from well-defined structures (A family ↔ I(0 0 1) configurations).

4.3. Discussion

4.3.1. Electronic transition energies

In order to reproduce small frequency shifts between A and B families of sites (40 cm^{-1} in fluorescence and 165 cm^{-1} in phosphorescence, i.e. only ∼0.1–0.2% of the calculated total energy of the doped argon samples), we explored the effects of the change in equilibrium geometries and guest–host potentials induced by electronic excitation of the guest molecule.

The naphthalene molecule is elongated along its short axis in the S_1 state [20] and along its long axis in the T_1 state [21,22]. The effect of geometry changes on interaction energies E_I with unchanged potentials was evaluated at 0.1 K (Table 3). The energy differences ($\Delta E_I = E_I^* - E_I$, Table 3) are nearly the same in the I(1 1 1) and II(1 1 1) configurations and slightly different in the I(0 0 1) one. The effects of S_1 and T_1 deformation are the same in the I(0 0 1) configuration but differ clearly in the X(1 1 1) ones where E_I^* is almost identical in T_1 and S_0 states in good agreement with a small $T_1 \rightarrow S_0$ transition frequency shift in the B-sites. This is due to the different constraints applied by the argon atoms of the lattice layer where the molecule is trapped.

The change of the guest–host potential may be represented in the first approximation as a modification of the Ar–C term, other terms being unchanged [2,5,22]. Interaction energies (E_I) were calculated for all three configurations using the Leutwyler's potential for the S_1 state [5]. No significant differences between these configurations were found, the red-shifts differ by not more than 15 cm^{-1}. The major part (94%) of the red-shift between the isolated molecule and the molecule embedded in the matrix comes from the contribution of the repulsive part of the LJ potential. This is consistent with the fact that in the simulated geometries we have obtained a cramped molecule with argon atoms displaced by repulsive forces. On the other hand, as the attractive part of the potential has a negligible contribution, it remains ill defined.

Another attempt was performed in order to obtain a better characterisation of the attractive part of the excited potential. In molecular complexes with rare gas atoms, the observed red-shifts of the $S_1 \leftrightarrow S_0$ transition are usually analysed in terms of dispersion energies. A theoretical method based on the SBEJ (Shalev, Ben-Horin, Even, Jortner) semi-empirical method [23] has been applied to van der Waals aggregates in order to evaluate such red-shifts in the electronic transitions [24]. Red-shifts are considered to result only of dispersion effects. They are directly evaluated using the second order perturbation calculation in the ground and excited states. The main parameter is fitted in order to reproduce the experimental red-shift in the naphthalene–argon 1-1 complex. The gas-to-matrix shift of $\sim$200 cm^{-1} calculated in this way is in a semi-quantitative agreement with its experimental value of 130 cm^{-1}, but does not vary significantly from one configuration to another [25]. This disagreement may be due to the neglect in the SBEJ method of variation of the repulsive potential between the ground and the excited states. Repulsive interactions are obviously more important in the rigid crystal lattice than in small clusters where there is no or only slight constraints on the surrounding rare gas atoms. They may produce a reduction of the red-shifts overestimated in the SBEJ treatment and a difference between configurations (site families). With the last method, the calculated red-shifts involve the dipolar moments μ of the electronic transitions. It cannot be applied to the $T_1 \leftrightarrow S_0$ transition where $\mu = 0$. Red-shifts experimentally exist in the matrix on this triplet–singlet transition and they strongly depend on the site family: other effects such as repulsion effects must be important.

With the isotropic potentials involved, there are no distinctions between the interactions with π or σ electrons on the carbon atoms, whereas we have underlined the differences on the interactions in the plane where the naphthalene is trapped and the interactions with the upper and lower layers. A more sophisticated treatment taking into account anisotropy of atom–atom attractive and repulsive interactions will be necessary for a correct description of site effects.

4.3.2. Intensity distribution in the $S_1 \leftrightarrow S_0$ spectra

The differences in the vibrational intensity distribution (feature (ii)) assuming the previous assignment of calculated configurations to site families will be discussed.

The intrinsic dipole moment μ_{01} of the $S_1 \leftrightarrow S_0$ transition is extremely weak (the intrinsic oscillator strength is less than 4×10^{-4} [1,26]) so that the transition intensity is mainly borrowed from higher excited electronic states by vibronic coupling (''Herzberg–Teller'' (HT) effect). In order to take into account the vibronic interactions, the electronic wave function $|S_1^*\rangle$ may be expressed as:

$$|S_1^*\rangle = |S_1\rangle + \sum_j \sum_n \frac{\langle S_n|(\partial H_0/\partial Q_j)|S_1\rangle}{[E(S_1) - E(S_n)]} Q_j |S_n\rangle, \tag{1}$$

where H_0 is the electronic hamiltonian of the isolated molecule and Q_j the normal coordinates of the vibrational modes. In the $S_1 \leftrightarrow S_0$ radiative transition moment, there are Franck–Condon (FC) contributions coming from the first term of Eq. (1), and HT contributions coming from the latter term of Eq. (1): $\langle v_0, S_0|\mu|v_1, S_1^*\rangle = FC + HT$ with

$$FC = \mu_{01}\langle v_0|v_1\rangle, \tag{2}$$

and

$$HT = \sum_j V_j \langle v_0|Q_j|v_1\rangle, \tag{3}$$

where $|v_n\rangle$ is the vibrational wave function in the S_n electronic state and V_j includes the vibronic coupling expressed in the second term of Eq. (1) and the dipole moment μ_{0n} of the $S_n \leftrightarrow S_0$ electronic transitions. $|v_n\rangle$ is a compact notation for the overall vibrational wave function and represents the product of all the vibrational wave functions $|n_i^n\rangle$ associated with the normal modes Q_i :

$$|v_j\rangle = \prod_i |n_i^j\rangle \quad \text{and} \quad \langle v_0|Q_i|v_1\rangle = \langle n_i^0|Q_i|n_i^1\rangle \prod_{k\neq i} \langle n_k^0|n_k^1\rangle. \tag{4}$$

The intensity of the non-totally symmetric vibronic bands results only from HT contributions involving excited states of B_{2u} symmetry, essentially the $S_2(1\,^1B_{2u})$ state—close in energy to S_1—and the $S_8(2\,^1B_{2u})$ state which has a high transition dipole moment to the ground state [26]. The intensity of 0_0^0 and vibronic bands involving totally symmetric modes results from interferences between FC and HT mechanisms [27–29], the last one being due essentially to the vibronic coupling with the $S_5(2\,^1B_{3u})$ state. Interference effects are known to be especially strong in the case of the 8 and 5 a_{1g} modes [29], their destructive behaviour producing in particular an almost absent 5_1^0 band in the fluorescence of the isolated molecule [27,30]. They are destructive in absorption when constructive in emission, and vice versa.

No significant modifications on the vibrational frequencies were observed from one site to another: the part of the potential explored in the involved vibrational motions is unchanged from one site to another. A rough estimate of the amplitudes of low-frequency vibrations shows a less important geometry modification compared to the difference of equilibrium geometries in the S_0, S_1 and T_1 states. One can then consider that there is no significant matrix effect on the vibrational terms involved in Eqs. (2) and (3), and probably also on the $\langle S_n|\partial H_0/\partial Q_j|S_1\rangle$ terms. Experiments exhibit an environment effect on the energies of the excited states. This is mainly a host effect ($E(S_2)$–$E(S_1) = 3070\ cm^{-1}$ in Ar and $2950\ cm^{-1}$ in Kr for example) but similar site effects are observed in argon and in krypton [1]: the influence of the environment on the energy differences involved in the HT contribution (cf. Eqs. (1) and (3)) cannot explain the feature (ii). It seems obvious that intensities of B_{2u}–A_{1g} transitions dependent on the large S_0–S_2 transition moment and the intrinsic strength of the S_1–S_2 coupling are less sensitive to environment effects than those of the weak B_{3u}–A_{1g} bands. Moreover, the large μ_{0n} moments of higher lying B_{3u} states are not so significantly modified by the medium as the intrinsic μ_{01} moment.

μ_{01} results from a difference between two strong contributions associated to two nearly degenerate electronic configurations. Slight changes in the electronic configurations or in their relative weight could produce strong effects on μ_{01}. Because of the interference between FC and HT contributions, a site effect on μ_{01} may induce different modifications of vibronic intensities for different a_{1g} vibrational modes and for the 0_0^0 band. The 0_0^0-band intensity is mainly due to the FC contribution, Eq. (2). In nitrogen matrices, the intensity ratio $R(0) = I(0)/I(8b_{1g})$ between the 0_0^0 band and the vibronic one involving the $8b_{1g}$ mode is significantly smaller than in the isolated molecule [1], in both absorption and emission: a decrease of μ_{01} in N_2 matrices could explain this behaviour. The intensity distribution of vibronic bands in the A family of sites is very similar to that of rigid matrices as nitrogen or *n*-pentane [1,31]. This similarity would result from

a similar decrease of μ_{01} in sites where the molecule is cramped between two crystallographic planes as in the I(0 0 1) configuration assigned to the A family of sites. In the X(1 1 1) configurations, the site symmetry is different and the value of μ_{01} may be increased in consequence of a non-symmetric deformation of the naphthalene molecule induced by the environment in the non-symmetric II(1 1 1) configuration.

In order to check whether a slight deformation of the molecule submitted to repulsive and attractive forces in the Ar lattice may induce a non-negligible change of the $S_1 \leftrightarrow S_0$ transition moment, ab initio complete active space CASSCF calculations have been carried out with the MOLCAS package [32], which allows the calculation, at the CASSCF level, of the transition dipole moment between the individually computed states, i.e. between non-orthogonal configurations. The complete active space contains 10 π-type molecular orbitals and the basis set is the CC-pVDZ basis set [33]. First of all, in the D_{2h} symmetry group, a geometry optimisation of the ground $1\,^1A_g$ state was performed at the CASSCF level of theory. In this geometry, the first excited state S_1, the $1\,^1B_{3u}$ state, was computed at the same level of theory and then a calculation of the $S_1 \leftrightarrow S_0$ transition moment was performed. The oscillator strength deduced from these results is $f = 1.456 \times 10^{-4}$, in agreement with experimental and other theoretical data [26,29,34]. Only in plane deformations have been tested, especially those that qualitatively correspond to the shape of the argon cavity in the II(1 1 1) configuration. They involve a slight distortion of one of the two cycles of naphthalene (less than 3° on angles, less than 0.05 Å on C–C distances) and stretching or in plane bending of H atoms. For each distorted geometry, CASSCF calculations with the same active π-type molecular orbitals space were carried out in the C_s group. In this case, the S_0 and S_1 states are of the same A′ symmetry, and correspond to the first two CI matrix roots. As the energy difference is large (~4 eV), the two states have been computed individually. A significant increase of the oscillator strength was obtained for two kinds of deformation. A displacement of C_4 (cf. Fig. 7 for notations) induces an increase of the μ_x component of the transition moment (the component of the $S_1 \leftrightarrow S_0$ transition moment) and a displacement of both C_4 and C_8 induces an increase of the μ_y component. For example, an oscillator strength of 3.9×10^{-4} was obtained for a displacement of C_4 involving a 3° increase of the $C_2C_1C_4$ and $C_4C_8C_{10}$ angles; a similar value—$f = 3.4 \times 10^{-4}$—was obtained via the other deformation involving a 3° increase of $C_2C_1C_4$ and $C_6C_{10}C_8$ angles. Such deformations induce an increase ΔE_0 of the ground state energy which must be smaller than the absolute value of the interaction energy E_I (Table 1) to make this deformation energetically allowed. Non-negligible ΔE_0 values were found in the two examples of deformations: 1890 and 4525 K respectively to be compared to $|E_I| \approx 7800$ K. We conclude that an increase of f can really be assumed in a non-symmetric site of the argon lattice but this increase cannot be larger than a factor 3. On the other hand, a decrease of f is possible under other environment conditions: such an evolution has been found in our tests with a distorted naphthalene having one cycle slightly smaller than the other one. In the experiments, the intensity ratio between the 0_0^0 bands of both families of sites is larger than 5. These calculations show this ratio may be explained by an increase of μ_{01} in the B-sites and a decrease of μ_{01} in the A-sites.

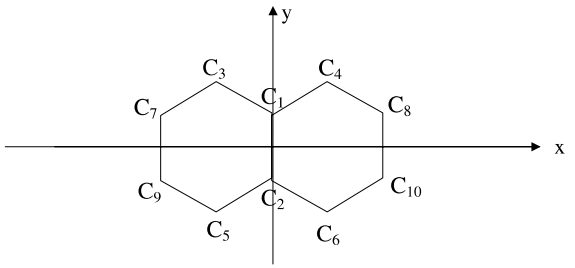

Fig. 7. Notations on the naphthalene orientation and on its carbon atoms used in the text.

4.4. Concluding remarks

All the observations can be qualitatively explained by the assignment: $A \leftrightarrow I(0\,0\,1)$ and $B \leftrightarrow X(1\,1\,1)$. Similar A and B families of sites

have been observed in krypton and methane matrices. Pair potentials involving these hosts are not very different from the case of argon: $\varepsilon(\mathrm{Kr–Kr}) = 1.3758 \times \varepsilon(\mathrm{Ar–Ar})$, $\varepsilon(\mathrm{CH_4–CH_4}) = 1.1395 \times \varepsilon(\mathrm{Ar–Ar})$ and $\sigma(\mathrm{Kr–Kr}) = 1.1692 \times \sigma(\mathrm{Ar–Ar})$, $\sigma(\mathrm{CH_4–CH_4}) = 1.1106 \times \sigma(\mathrm{Ar–Ar})$ [35]. Using the Lorentz and Berthelot combination rules [35], it is possible to deduce host-C and host-H pair potentials. In any case, the guest–host interaction will remain less important than the host–host interaction so that the favoured trapping sites will also correspond to small cavities. Lattice parameters of krypton and methane fcc crystals are only slightly larger than the argon ones: nearest neighbours distance is 4.0 Å in Kr and 4.16 Å in CH_4. As in the case of argon, the interaction between the naphthalene molecule and the matrix will be mainly repulsive. One can then assume that the main trapping sites are similar in both hosts and in argon, implying similar effects on the dynamics of excited naphthalene molecules [1].

5. Conclusion

Our MD calculations simulate the gas deposition on a cold surface, with time parameters reflecting as well as possible the realistic conditions. Three main configurations were obtained. The naphthalene is trapped either in the (0 0 1) plane or in the (1 1 1) plane and replaces either four argon atoms (in both planes) or five argon atoms (in the (1 1 1) case). Small trapping cavities are obtained because the C–Ar interaction is weaker than the Ar–Ar one: the replacement of argon atoms by the guest molecule in the lattice is energetically unfavourable.

Two families of sites are assigned to the two different configurations with a molecule in the (1 1 1) or (0 0 1) crystallographic planes. This assignment is based on the relation between spectroscopic and dynamic properties of the guest molecule and its perturbation in a given type of cavity. In the present state of art, it is not possible to give a more quantitative description of the environment effects on the behaviour of the excited molecule in absence of a better knowledge of the host–guest potential in the case of the electronic excitation. It concerns in particular the repulsive part of the excited state potential which plays a more important role in matrices than in small free clusters. Note also that in our simulation of matrix formation, the molecules were considered as rigid, whereas their properties are sensitive to small deformations.

Acknowledgements

We gratefully acknowledge A. Tramer for helpful and fruitful discussions.

References

[1] C. Crépin, A. Tramer, Chem. Phys. 272 (2001) 227.
[2] J. Najbar, A.M. Turek, T.D.S. Hamilton, J. Lumin. 26 (1982) 281;
A.M. Turek, J. Najbar, Acta Phys. Polon. A 58 (1980) 317.
[3] R. Fraenkel, D. Schweke, Y. Haas, F. Molnar, D. Horinek, B. Dick, J. Phys. Chem. A 104 (2000) 3786.
[4] A.J. Cruz, G.E. Lopez, J. Chem. Phys. 104 (1996) 4301.
[5] T. Troxler, S. Leutwyler, J. Chem. Phys. 99 (1993) 4363;
T. Troxler, S. Leutwyler, J. Chem. Phys. 95 (1991) 4010.
[6] M.-P. Gaigeot, P. de Pujo, V. Brenner, Ph. Millié, J. Chem. Phys. 106 (1997) 9155.
[7] K.F. Niebel, J.A. Venables, in: M.L. Klein, J.A. Venables (Eds.), Rare Gas Solids, Academic Press, New York, 1976.
[8] H.J.C. Berendsen, J.P.M. Postma, W.F. Van Gunsteren, A. Di Nola, J.R. Haak, J. Chem. Phys. 81 (1984) 3684.
[9] P. de Pujo, J.-M. Mestdagh, J.-P. Visticot, J. Cuvellier, P. Meynadier, O. Sublemontier, A. Lallement, J. Berlande, Z. Phys. D 25 (1993) 357.
[10] Tables of Interatomic Distances and Configurations in Molecules and Ions, The Chemical Society, Burlington House, 1958.
[11] S.M. Beck, D.E. Powers, J.B. Hopkins, R.E. Smalley, J. Chem. Phys. 73 (1980) 2019.
[12] H. Gattermann, M. Stockburger, J. Chem. Phys. 63 (1975) 4541.
[13] K.C. Lin, S.H. Lin, Mol. Phys. 21 (1971) 1105.
[14] K. Sohlberg, D.R. Yarkony, J. Chem. Phys. 107 (1997) 7690.
[15] S. Matsika, R.M. Pitzer, J. Phys. Chem. A 102 (1998) 1652.
[16] G.J. Hoijtink, Mol. Phys. 3 (1960) 67.
[17] R. Pellow, M. Vala, J. Chem. Phys. 90 (1989) 5612.
[18] J.N. Murrell, Mol. Phys. 3 (1960) 319.
[19] J.M.O. Matos, B.O. Roos, Theor. Chim. Acta 74 (1988) 363.
[20] K.K. Innes, in: E.C. Lim (Ed.), Excited States, vol. 2, Academic Press, New York, 1975, p. 1;
G.S. Jas, K. Kuczera, Chem. Phys. 214 (1997) 229.

[21] S. Kudoh, M. Takayanagi, M. Nakata, J. Mol. Struct. 475 (1999) 253.
[22] J. Najbar, A.M. Turek, Chem. Phys. Lett. 73 (1980) 536.
[23] E. Shalev, N. Ben-Horin, U. Even, J. Jortner, J. Chem. Phys. 96 (1992) 1848;
E. Shalev, N. Ben-Horin, U. Even, J. Jortner, J. Chem. Phys. 95 (1991) 3147.
[24] B. Bouvier, DEA report, Université Paris-Sud, 1999.
[25] B. Bouvier, V. Brenner, private communication.
[26] M. Rubio, M. Merchan, E. Orti, B.O. Roos, Chem. Phys. 179 (1994) 395.
[27] M. Stockburger, H. Gatterman, W. Klusman, J. Chem. Phys. 63 (1975) 4519, 4529.
[28] G. Holneicher, J. Wolf, Ber. Bunsenges. Phys. Chem. 99 (1995) 366, and reference therein.
[29] F. Negri, M.Z. Zgierski, J. Chem. Phys. 104 (1996) 3486, and reference therein.
[30] S.M. Beck, J.B. Hopkins, D.E. Powers, R.E. Smalley, J. Chem. Phys. 74 (1981) 43.
[31] J.J. Dekkers, G.Ph. Hoornweg, C. Maclean, N.H. Velthorst, Chem. Phys. 5 (1974) 393.
[32] K. Andersson, M.R.A. Blomberg, M.P. Fülscher, G. Karlström, R. Lindh, P.Å. Malmqvist, P. Neogràdy, J. Olsen, B.O. Roos, A.J. Sadlej, M. Schütz, L. Seijo, L. Serrano-Andrès, P.E.M. Siegbahn, P.O. Widmark, "MOLCAS Version 4.1", Lund University, Sweden, 1997.
[33] T.H. Dunning Jr., J. Chem. Phys. 90 (1989) 1007.
[34] G.A. George, G.C. Morris, J. Mol. Spectrosc. 26 (1968) 67.
[35] G.C. Maitland, M. Rigby, E.B. Smith, W.A. Wakeham, Intermolecular Forces: Their Origin and Determination, Oxford University Press, Oxford, 1987.